High-Temperature Hall Effect Sensor Based on Epitaxial Graphene on High-Purity Semiinsulating 4H-SiC

Tymoteusz Ciuk, Beata Stanczyk, Krystyna Przyborowska, Dariusz Czolak, Artur Dobrowolski, Jakub Jagiello, Wawrzyniec Kaszub, Michal Kozubal, Roman Kozlowski, and Pawel Kaminski

***Abstract*— In this report, we demonstrate a novel high-temperature Hall effect sensor that is based on quasi-free-standing monolayer graphene epitaxially grown on high-purity semiinsulating (SI) on-axis 4H-SiC(0001) substrate in a chemical vapor deposition process. To ensure statistical perspective, characteristics of 23 elements are determined as a function of temperature ranging from 300 to 770 K. Passivated with a 100-nm-thick atomic-layer-deposited aluminum oxide, the sensor offers current-mode sensitivity of 80 V/AT with thermal stability of −0.02%/K within the range between 300 and 573 K, and −0.06%/K between 573 and 770 K. The sensor's room-temperature output voltage is monitored in the magnetic field from −300 to +300 mT and its offset voltage at 0 T is assessed. Its high-temperature electrical properties are explained through a double-carrier transport involving spontaneous-polarization-induced holes in the graphene layer and thermally activated electrons emitted from a deep acceptor level related to silicon vacancy $V_{Si}^{1-/2-}$ occupying the *k* site of the 4H-SiC lattice. The sensor is compared with a previously reported one on vanadium-compensated SI on-axis 6H-SiC(0001). The new sensor's applicability to magnetic field detection at high temperatures is verified.**

***Index Terms*— Graphene, Hall effect sensor, high temperature.**

Manuscript received March 15, 2019; revised April 24, 2019; accepted May 2, 2019. Date of publication May 23, 2019; date of current version June 19, 2019. This work was supported in part by the National Centre for Research and Development through the Project "Graphene on Silicon Carbide Devices for Magnetic Field Detection in Extreme Temperature Conditions" under Grant LIDER 0168/L-8/2016 and Project "Technologies of Semiconductor Materials for High Power and High Frequency Electronics" under Grant TECHMATSTRATEG1/346922/4/NCBR/2017 and in part by the European Union's Horizon 2020 Research and Innovation Programme under Grant 785219. The review of this paper was arranged by Editor G. L. Snider.
(Corresponding author: Tymoteusz Ciuk.)

T. Ciuk, B. Stanczyk, K. Przyborowska, D. Czolak, W. Kaszub, R. Kozlowski, and P. Kaminski are with the Institute of Electronic Materials Technology, 01-919 Warsaw, Poland (e-mail: tymoteusz.ciuk@itme.edu.pl).

A. Dobrowolski and J. Jagiello are with the Institute of Electronic Materials Technology, 01-919 Warsaw, Poland, and also with the Faculty of Physics, University of Warsaw, 02-093 Warsaw, Poland.

M. Kozubal is with the Institute of Electronic Materials Technology, 01-919 Warsaw, Poland, and also with VIGO System S.A., 05-850 Warsaw, Poland.

Color versions of one or more of the figures in this paper are available online at http://ieeexplore.ieee.org.

Digital Object Identifier 10.1109/TED.2019.2915632

I. Introduction

PLANAR Hall effect sensors had been initially fabricated in thin films, e.g., 20-nm-thick permalloy [1]. With the advent of the era of truly 2-D materials, graphene has become first choice for magnetic field detection. Reported technologies of graphene-based Hall effect elements include: graphene grown on copper [2], [3] or platinum [4], [5] and transferred onto SiO_2/Si, exfoliated or copper grown graphene transferred onto hexagonal boron nitride [6], [7], epitaxial graphene on SiC [8], [9], and epitaxial chemical vapor deposited graphene on SiC [10]–[12].

Epitaxial CVD graphene on semiinsulating (SI) silicon carbide has already been verified as a likely material for the future graphene applications. Reported monolithic microwave integrated circuits (MMICs) [13]–[15] show its promise in millimeter-wave electronics. They take advantage of graphene's charge carriers mobility. Here, we infer that another property, namely, the unprecedented thermal stability of its transport properties may bring it closer to application.

Recently, we have published on a Hall effect sensor fabricated on quasi-free-standing (QFS) monolayer graphene grown on vanadium-compensated SI on-axis 6H-SiC(0001) substrate in an epitaxial chemical vapor deposition (CVD) process [16]. We demonstrated that when passivated with a 100-nm-thick aluminum oxide layer, the sensor's current-mode sensitivity is

$$S_I = \left(\frac{\partial U_{\mathrm{Hall}}}{\partial B}\right)/I = 1/p_s e[\mathrm{V/AT}] \quad (1)$$

where U_{Hall} is the Hall voltage, B is the magnetic field, I is the driving current, p_s is the sheet charge carrier concentration, and e is the unit charge, reached ∼140 V/AT with thermal stability of −0.01%/K within the range between 80 and 300 K and of −0.02%/K between 300 and 573 K. Following these characteristics, we suggested that the sensor is complementary to CMOS (180 V/AT) [17], GaAs (160 V/AT), InAs (330 V/AT), and InSb (2000 V/AT) [18] technologies as its inferior sensitivity is compensated by broader range of operation (already referred to as high-temperature CMOS sensors are limited to 473 K [19], GaAs and InAs sensors to 398 K, and InSb sensors to 383 K [18]).

In the range between 573 and 770 K, the stability of that sensor's current mode-sensitivity dropped to −0.26%/K and

0018-9383 © 2019 IEEE. Translations and content mining are permitted for academic research only. Personal use is also permitted, but republication/redistribution requires IEEE permission. See http://www.ieee.org/publications_standards/publications/rights/index.html for more information.

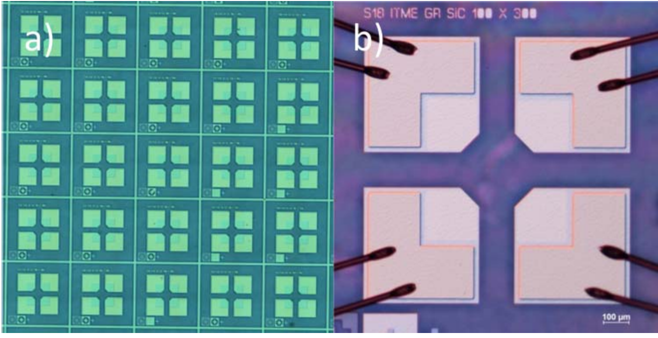

Fig. 1. (a) Nomarski interference contrast image of 25 Hall effect elements made from QFS hydrogen-intercalated monolayer graphene grown in an epitaxial CVD process on HP SI on-axis 15 mm × 15 mm 4H-SiC (0001) substrate and passivated with a 100-nm-thick atomic-layer-deposited aluminum oxide layer synthesized at 670 K from TMA and deionized water. (b) Optical image of a single wire-bonded 1.6 mm × 1.6 mm element.

its reversible decrease was explained through a double-carrier transport involving spontaneous-polarization-induced holes in the graphene layer and thermally activated electrons from a deep acceptor level of vanadium located in the hexagonal (h) site of the 6H-SiC lattice. It was suggested that if the vanadium-compensated substrate was replaced with a high-purity (HP) undoped one, the thermal stability of the sensor could improve significantly.

In this paper, we present an advanced aluminum-oxide-passivated Hall effect sensor that is based on QFS-monolayer graphene grown in an industrial epitaxial CVD technology on HP SI on-axis 4H-SiC(0001). We define its applicability to high-temperature magnetic field detection and use it to study charge carriers transport between 300 and 770 K.

II. Experimental Details

A. Graphene Epitaxy and the Hall Effect Sensor Technology

QFS graphene has been obtained through hydrogen atom intercalation of the sole buffer layer epitaxially grown on HPSI on-axis 15 mm × 15 mm 4H-SiC (0001) substrate (Cree Inc.) in a hot-wall Aixtron VP508 reactor with the CVD method [20].

The sensor features a symmetrical cross-shaped 1.6 mm × 1.6 mm *van der Pauw* structure. Its processing cycle is based on a classical optical lithography and Ti/Au (10 nm/60 nm) ohmic contacts. The sensor is passivated with a 100-nm-thick aluminum oxide layer synthesized from trimethylaluminum [TMA, $Al_2(CH_3)_6$] and deionized water at 670 K in a high-temperature atomic layer deposition (ALD) process in the 4-in Picosun R200 Advanced reactor. Fig. 1 illustrates 25 elements on the 11 mm × 11 mm working area of the 15 mm × 15 mm 4H-SiC(0001) substrate and a single wire-bonded 1.6 mm × 1.6 mm mm element.

For the hereafter explained reasons, one of the 25 sensors depicted in Fig. 1 had the aluminum oxide passivation etched away with ammonium-fluoride-buffered hydrofluoric acid leaving unpassivated graphene, and another one had not only the passivation removed, but also the graphene layer fully etched with an oxygen plasma, so that bare 4H-SiC (0001) remained between the ohmic contacts. Next, all 1.6 mm × 1.6 mm elements were mounted and bonded to custom-made 10 mm × 10 mm sapphire holders equipped with four Cr/Au (100 nm/20 nm) corner contacts to enable electrical characterization.

B. Electrical Characterization

In order to assess the elements' sheet charge carrier concentration p_s [cm^{-2}], mobility μ_p [cm^2/Vs], sheet resistance R_s[Ω/sq], and current-mode sensitivity S_I[V/AT] as a function of temperature in the range between 300 and 770 K, all were fed with I = 1-mA direct current and characterized with a 0.556 T Ecopia AHT55T5 automated Hall effect measurement system. Their room-temperature output voltage was monitored in the magnetic field between −300 and +300 mT of a WPsensors EP-001electromagnet.

III. Experimental Results and Discussion

A. Current-Mode Sensitivity and Offset Voltage

At room temperature (300 K), the 23 elements' arithmetical mean current-mode sensitivity is $S_{\text{Imean}} \approx 83$ V/AT with the standard deviation $\sigma \approx 3.8$ V/AT. It is lower than in the above-cited publications on graphene grown on copper and transferred onto SiO_2/Si (310 V/AT [2], 2540 V/AT [3]), graphene grown on platinum and transferred onto SiO_2/Si (800 V/AT [4], 1200 V/AT [5]), exfoliated or copper grown graphene transferred onto hexagonal boron nitride (5700 V/AT [6], 1986 V/AT [7]), epitaxial graphene on SiC (310 V/AT [8], 1000 V/AT [9]) yet higher than in the permalloy (30 V/AT [1]) and consistent with other reports on epitaxial CVD graphene on SiC (83 V/AT [11], 50 V/AT [12]). At 573 K, the elements offer $S_{\text{Imean}} \approx 79$ V/AT with $\sigma \approx 2.9$ V/AT and these values are greatly stable up to 770 K, where $S_{\text{Imean}} \approx 67$ V/AT and $\sigma \approx 4.5$ V/AT (Fig. 2). Importantly for application, the curves are reproducible and no degradation of the Ti/Au contacts is observed even at 770 K. The relatively low value of current-mode sensitivity stems from the relatively high charge carrier concentration. As described in the following, it is an intrinsic property of QFS graphene on hexagonal SiC and its consistency with the theoretical predictions only proves in favor of our technology. The uniformity of hole concentration narrows the data spread and increases the yield. On the other hand, hole concentration in transferred graphene is greatly related to polymer residue on its surface [21], and therefore, it is random to some extent.

In the range between 300 and 573 K, the arithmetical mean thermal stability defined as

$$\frac{\left(S_{\text{Imean}}^{T_2} - S_{\text{Imean}}^{T_1}\right)}{S_{\text{Imean}}^{T_1}(T_2 - T_1)} \times 100\% \tag{2}$$

where $T_1 = 300$ K and $T_2 = 573$ K, is negative and equals −0.02%/K, which is exactly the previously reported value for passivated graphene on vanadium-compensated SI on-axis 6H-SiC. However, between 573 and 770 K, it drops to −0.06%/K only, as opposed to the −0.26%/K for 6H-SiC (0001) [16].

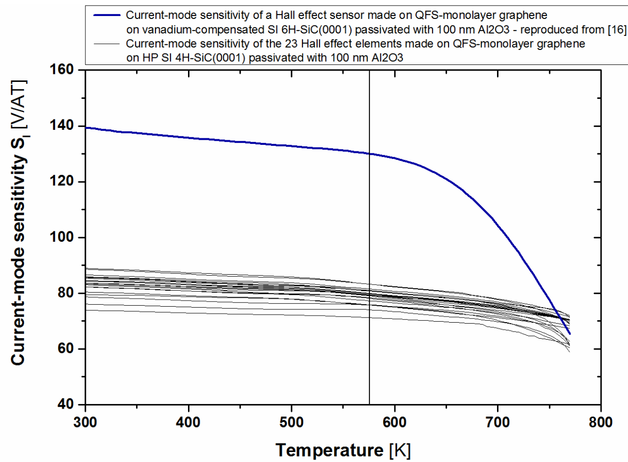

Fig. 2. Current-mode sensitivity of 23 Hall effect elements as a function of temperature (black lines). Blue: reproduction of a single sensor fabricated in the same technology on vanadium-compensated SI 6H-SiC (0001) [16].

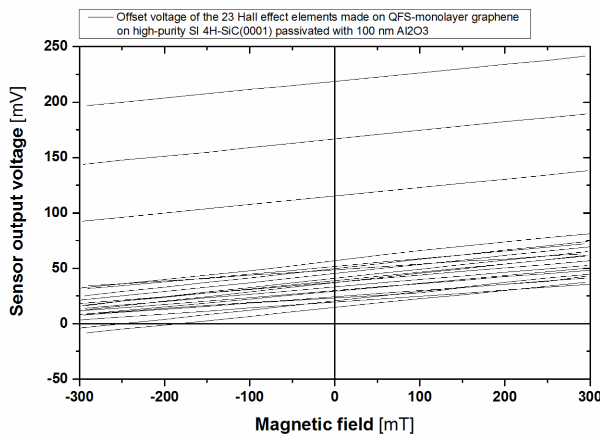

Fig. 3. Output voltage in the perpendicular magnetic field between $B = -300$ mT and $B = +300$ mT of the 23 Hall effect elements fed with $I = 1$-mA direct current. Visible is the offset voltage range at $B = 0$ T.

We had previously shown that the characteristic and inherent morphology of SiC surface marked with terraces and step edges introduces significant anisotropy into graphene's sheet resistance [22] and promotes an anisotropic offset voltage [23], [24]. This voltage occurs between the output electrodes and adds to the Hall voltage, thus constituting an operating point of the sensor in zero magnetic field. When fed with $I = 1$ mA direct current and swept from -300 mT and $+300$ mT, the sensors revealed that the offset voltage is typically below $U_{\text{out}} \approx 50$ mV but occasionally up to 200 mV (Fig. 3), even though the processing conditions were uniform for all sensors. This observation implies that the step-edge-induced offset voltage may be a significant and unavoidable yield-limiting factor.

B. Transport Properties as a Function of Temperature

In order to explain the physical phenomena underlying the current-mode sensitivity profiles, the 23 passivated elements and the element that had the passivation removed were characterized in a static magnetic field of 0.556 T in the temperature range between 300 and 770 K. The one with only bare 4H-SiC (0001) left was analyzed in a narrower range between 470 and 770 K.

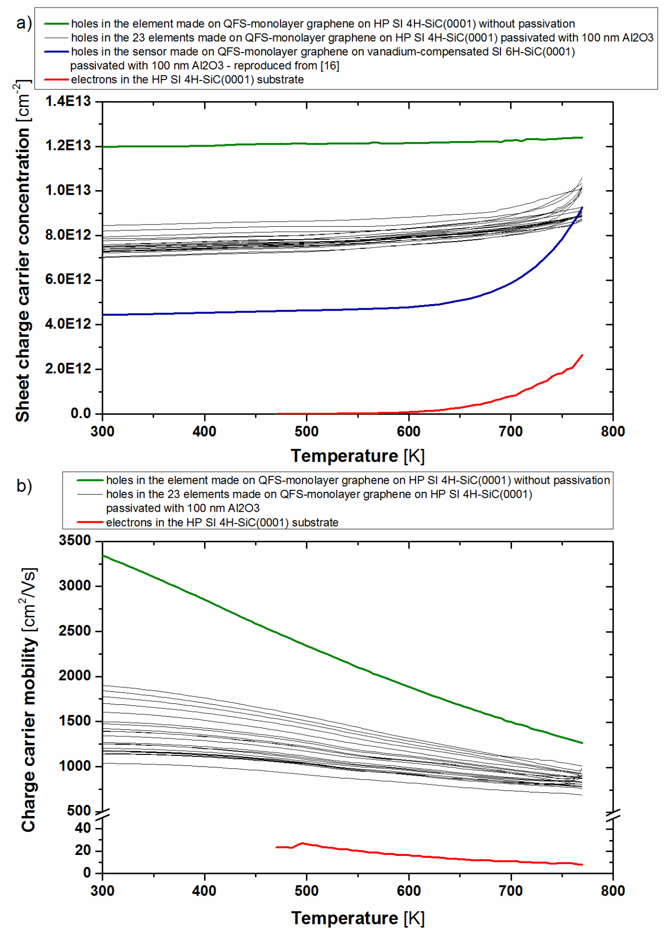

Fig. 4. Temperature profile of (a) sheet charge carrier concentration and (b) mobility as a function of temperature measured in the 25 Hall effect elements. Green: element that had the passivation etched away. Black: 23 passivated elements. Blue: reproduction of a single sensor fabricated in the same technology on vanadium-compensated SI 6H-SiC (0001) [16]. Red: element the had the passivation and the graphene layer removed.

Following our expectations, charge transport measured in the sensor that had the passivation removed is of p-type and the hole concentration $p_S = 1.20 \times 10^{13}$ cm^{-2} proves consistent with the theoretically predicted $p_S^{4\text{H}} \approx 1.2 \times 10^{13}$ cm^{-2} for as-grown QFS epitaxial graphene on 4H-SiC (0001) [23]–[27]. Its value remains almost unaffected by the temperature rise and reaches $p_S = 1.24 \times 10^{13}$ cm^{-2} at 770 K.

In the 23 passivated elements, the polarization effect of the positively charged oxygen vacancies present in the 100-nm-thick aluminum oxide layer [28] suppresses the influence of the spontaneous polarization of SiC and pins the arithmetical mean hole concentration at $p_{\text{Smean}} \approx 7.5 \times 10^{12}$ cm^{-2} with $\sigma \approx 3.6 \times 10^{11}$ cm^{-2} at 300 K, $p_{\text{Smean}} \approx 7.9 \times 10^{12}$ cm^{-2} with $\sigma \approx 2.9 \times 10^{11}$ cm^{-2} at 573 K, and $p_{\text{Smean}} \approx 9.4 \times 10^{12}$ cm^{-2} with $\sigma \approx 6.5 \times 10^{11}$ cm^{-2} at 770 K [Fig. 4(a)]. The decrease in the room-temperature hole concentration to approximately 60% of its value without passivation is quantitatively consistent with our previous report on a single sensor fabricated

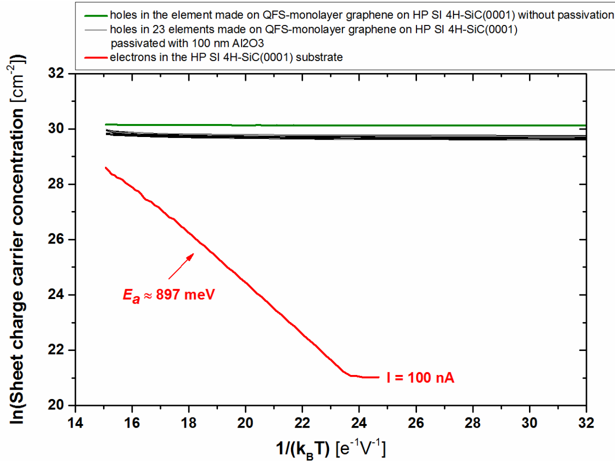

Fig. 5. Natural logarithm of sheet charge carrier concentration plotted against the inverse of $k_B T$ in the range between 300 and 770 K measured in the 23 passivated elements (black lines), the element that had the passivation etched away (green line) and the element the had the passivation and the graphene layer removed (red line).

in the same technology on vanadium-compensated SI 6H-SiC (0001) [16].

It is also evident from Fig. 4(b) that the presence of the aluminum oxide passivation suppresses the hole mobility. In the element that had the passivation removed the room-temperature hole mobility $\mu = 3344$ cm^2/Vs and drops to $\mu = 1995$ cm^2/Vs at 573 K, and $\mu = 1260$ cm^2/Vs at 770 K. In the 23 passivated elements, the arithmetical mean hole mobility equals $\mu_{\text{mean}} \approx 1388$ cm^2/Vs with $\sigma \approx 251$ cm^2/Vs at 300 K, $\mu_{\text{mean}} \approx 1079$ cm^2/Vs with $\sigma \approx 148$ cm^2/Vs at 573 K, and at $\mu_{\text{mean}} \approx 859$ cm^2/Vs with $\sigma \approx 81$ cm^2/Vs at 770 K.

The experimentally observed thermal stability of p_s in a wide range of temperatures is in contrast to the steep rise above approximately 620 K that had been previously observed in 6H-SiC [16] and explained through a double-carrier system involving holes in the graphene layer and electrons in the SiC substrate. However, since the value of the spontaneous polarization of 4H-SiC is constant in the range between 0 and 120 meV (~1400 K) [27], the moderate rise of p_s in the upper range of temperatures suggests the presence of a similar, yet less prominent effect in 4H-SiC.

Due to its higher electrical resistance, the element with only bare 4H-SiC (0001) left was fed with direct current $I = 100$ nA. At room temperature, the resistivity of SI 4H-SiC substrate proved very high (of the order of $10^8\Omega$ cm). However, starting from 470 K, a population of hardly mobile electrons (Fig. 4) appeared following the exponent of the Arrhenius equation $\exp(-E_a/k_B T)$, where E_a is the activation energy, k_B is Boltzmann's constant, and T is the absolute temperature. Its natural logarithm plotted against the inverse of $k_B T$ (Fig. 5) revealed $E_a \approx 897$ meV. Based on the literature, the intrinsic deep level defects present in the upper half of the bandgap of HP SI 4H-SiC typically span the range between $E_a \approx 0.45$ eV and $E_a \approx 1.65$ eV [29]–[32]. We attribute $E_a \approx 897$ meV to a silicon vacancy $V_{\text{Si}}^{1-/2-}$ in the k site [33] as it was identified by high-resolution photoinduced transient spectroscopy (HRPITS) measurements. We infer that as the temperature rises, the Fermi level in the HP SI 4H-SiC substrate shifts toward the middle of the bandgap located at E_c–1.63 eV, where E_c is the conduction band minimum, and crosses the acceptor level at E_c–897 meV. The change in the silicon vacancy charge state from V^{2-} to V^- is followed by the experimentally observed electron emission.

C. Role of the SiC Substrate

At room temperature, the experimentally confirmed spontaneous-polarization-induced hole concentration in QFS graphene on SI SiC is consistent with the theoretical predictions and equals $p_S^{4\text{H}} \approx 1.2 \times 10^{13}$ cm^{-2} and $p_S^{6\text{H}} \approx 7.5 \times 10^{12}$ cm^{-2} [16]. Suppressed with the polarization effect of the positively charged oxygen vacancies present in the 100-nm-thick aluminum oxide passivation, it drops to 60% of its initial value and equals $p_S^{4\text{H}} \approx 7.5 \times 10^{12}$ cm^{-2} and $p_S^{6\text{H}} \approx 4.6 \times 10^{12}$ cm^{-2} [16], which translates into the current-mode sensitivity of $\text{S}_\text{I}^{4\text{H}} \approx 83$ V/AT and $\text{S}_\text{I}^{6\text{H}} \approx 140$ V/AT [16]. In the range between 300 and 573 K, both the HP SI 4H-SiC(0001) and the vanadium-compensated SI 6H-SiC (0001) platforms offer comparable thermal stability, yet the latter one is almost twice as sensitive.

Above 573 K, the electrical properties of the Hall effect sensors are governed by a double-carrier transport involving holes in the graphene layer and thermally activated electrons in the bulk of the substrate; therefore, they are determined by the SiC defect structure.

The quantitative difference between the two substrates lies in the temperature at which sheet concentration of the thermally activated electrons becomes measurable (470 K for 4H-SiC and 420 K for 6H-SiC) and in the temperature at which it becomes comparable with hole concentration in graphene. It has already been observed that in the passivated QFS graphene on vanadium-compensated SI 6H-SiC (0001) [16], this occurs at 650 K. In this report, the temperature range proved insufficient for such observation; however, it may be anticipated from Fig. 5 that in passivated QFS graphene on HP SI 4H-SiC(0001), the corresponding temperature is above 800 K.

The discrepancy between the two substrates stems from the fact that the sheet concentration of the thermally activated electrons is on average 20 times smaller in HP SI 4H-SiC than in vanadium-compensated SI 6H-SiC. Therefore, above 573-K thermal stability proves in favor of HP SI 4H-SiC (0001). As a result, the two substrates offer a characteristic interchangeability of current-mode sensitivity and thermal stability.

IV. Conclusion

In this report, we have demonstrated a novel Hall effect sensor made from QFS hydrogen-intercalated monolayer graphene epitaxially grown on HP SI on-axis 4H-SiC (0001) substrate in a CVD process. Passivated with a 100-nm-thick atomic-layer-deposited aluminum oxide, the sensor offers current-mode sensitivity of 80 V/AT with thermal stability

of −0.02%/K between 300 and 573 K, and −0.06%/K between 573 and 770 K.

It was found that the sensor's high-temperature electrical properties are governed by a double-carrier transport involving spontaneous-polarization-induced holes in the graphene layer and thermally activated electrons emitted from a silicon-vacancy-related deep acceptor level due to the change of its charge state from V^{2-} to V.

In the range between 573 and 770 K, the thermal stability of sensor's current-mode sensitivity is superior to the previously reported Hall effect sensor on vanadium-compensated SI 6H-SiC (0001); however at 770 K, both technologies equalize. The unmatched stability opens field for novel applications in high-temperature magnetic field detection.

References

[1] L. Ejsing, M. F. Hansen, A. K. Menon, H. A. Ferreira, D. L. Graham, and P. P. Freitas, "Planar Hall effect sensor for magnetic micro- and nanobead detection," *App. Phys. Lett.*, vol. 84, no. 23, pp. 4729–4731, 2004.

[2] C. C. Tang, M. Y. Li, L. J. Li, C. C. Chi, and J. C. Chen, "Characteristics of a sensitive micro-Hall probe fabricated on chemical vapor deposited graphene over the temperature range from liquid-helium to room temperature," *Appl. Phys. Lett.*, vol. 99, no. 11, 2011, Art. no. 112107.

[3] D. Izci, C. Dale, N. Keegan, and J. Hedley, "The construction of a Graphene Hall effect magnetometer," *IEEE Sensors J.*, vol. 18, no. 23, pp. 9534–9541, Dec. 2018.

[4] H. Xu, L. Huang, Z. Zhang, B. Chen, H. Zhong, and L.-M. Peng, "Flicker noise and magnetic resolution of graphene Hall sensors at low frequency," *Appl. Phys. Lett.*, vol. 103, no. 11, 2013, Art. no. 112405.

[5] H. Xu *et al.*, "Batch-fabricated high-performance graphene Hall elements," *Sci. Rep.*, vol. 3, Feb. 2013, Art. no. 1207.

[6] J. Dauber *et al.*, "Ultra-sensitive Hall sensors based on graphene encapsulated in hexagonal boron nitride," *App. Phys. Lett.*, vol. 106, no. 19, 2015, Art. no. 193501.

[7] M.-K. Joo *et al.*, "Large-scale graphene on hexagonal-BN Hall elements: Prediction of sensor performance without magnetic field," *ACS Nano*, vol. 10, no. 9, pp. 8803–8811, 2016.

[8] V. Panchal, K. Cedergren, R. Yakimova, A. Tzalenchuk, S. Kubatkin, and O. Kazakova, "Small epitaxial graphene devices for magnetosensing applications," *J. Appl. Phys.*, vol. 111, Nov. 2012, Art. no. 07E509.

[9] R. K. Rajkumar, A. Asenjo, V. Panchal, A. Manzin, Ó. Iglesias-Freire, and O. Kazakova, "Magnetic scanning gate microscopy of graphene Hall devices (invited)," *J. Appl. Phys.*, vol. 115, Dec. 2014, Art. no. 172606.

[10] O. Petruk *et al.*, "Sensitivity and offset voltage testing in the Hall-effect sensors made of graphene," in *Recent Advances in Automation, Robotics and Measuring Techniques*, vol. 267. Cham, Switzerland: Springer, 2014, pp. 631–640.

[11] T. Ciuk *et al.*, "Low-noise epitaxial graphene on SiC Hall effect element for commercial applications," *Appl. Phys. Lett.*, vol. 108, Jun. 2016, Art. no. 223504.

[12] M. Kachniarz *et al.*, "Quasi-free-standing bilayer graphene Hall-effect sensor," *IEEE Trans. Magn.*, vol. 55, no. 1, Jan. 2019, Art. no. 4000204.

[13] O. Habibpour, Z. S. He, W. Strupinski, N. Rorsman, and H. Zirath, "Wafer scale millimeter-wave integrated circuits based on epitaxial graphene in high data rate communication," *Sci. Rep.*, vol. 7, Feb. 2017, Art. no. 41828.

[14] O. Habibpour *et al.*, "A W-band MMIC resistive mixer based on epitaxial graphene FET," *IEEE Microw. Wireless Compon. Lett.*, vol. 27, no. 2, pp. 168–170, Feb. 2017.

[15] O. Habibpour *et al.*, "Graphene FET gigabit ON–OFF keying demodulator at 96 GHz," *IEEE Electron Devices Lett.*, vol. 37, no. 3, pp. 333–336, Mar. 2016.

[16] T. Ciuk *et al.*, "Thermally activated double-carrier transport in epitaxial graphene on vanadium-compensated 6H-SiC as revealed by Hall effect measurements," *Carbon*, vol. 139, pp. 776–781, Nov. 2018.

[17] P. Kejik, G. Boero, M. Demierre, and R. S. Popovic, "An integrated micro-Hall probe for scanning magnetic microscopy," *Sens. Actuators A, Phys.*, vol. 129, pp. 212–215, May 2006.

[18] *Asahi Kasei Microdevices Corporation*. Accessed: Mar. 15, 2019. [Online]. Available: https://www.akm.com

[19] Micropac Industries. Accessed: Mar. 15, 2019. [Online]. Available: https://www.micropac.com

[20] W. Strupinski *et al.*, "Graphene epitaxy by chemical vapor deposition on SiC," *Nano Lett.*, vol. 11, no. 4, pp. 1786–1791, 2011.

[21] T. Ciuk *et al.*, "Properties of chemical vapor deposition graphene transferred by high-speed electrochemical delamination," *J. Phys. Chem. C*, vol. 117, no. 40, pp. 20833–20837, 2013.

[22] T. Ciuk *et al.*, "Step-edge-induced resistance anisotropy in quasi-free-standing bilayer chemical vapor deposition graphene on SiC," *J. Appl. Phys.*, vol. 116, Sep. 2014, Art. no. 123708.

[23] T. Ciuk and W. Strupinski, "Statistics of epitaxial graphene for Hall effect sensors," *Carbon*, vol. 93, pp. 1042–1049, Nov. 2015.

[24] T. Ciuk, P. Caban, and W. Strupinski, "Charge carrier concentration and offset voltage in quasi-free-standing monolayer chemical vapor deposition graphene on SiC," *Carbon*, vol. 101, pp. 431–438, May 2016.

[25] J. Ristein, S. Mammadov, and T. Seyller, "Origin of doping in quasi-free-standing graphene on silicon carbide," *Phys. Rev. Lett.*, vol. 108, Jun. 2012, Art. no. 246104.

[26] S. Mammadov *et al.*, "Polarization doping of graphene on silicon carbide," *2D Mater.*, vol. 1, no. 3, 2014, Art. no. 035003.

[27] J. Slawinska, H. Aramberri, M. C. Muñoz, and J. I. Cerdá, "Ab initio study of the relationship between spontaneous polarization and p-type doping in quasi-freestanding graphene on H-passivated SiC surfaces," *Carbon*, vol. 93, pp. 88–104, Oct. 2015.

[28] M. Choi, A. Janotti, and C. G. Van de Walle, "Native point defects and dangling bonds in α-Al_2O_3," *J. Appl. Phys.*, vol. 113, 2013, Art. no. 044501.

[29] T. Dalibor *et al.*, "Deep defect centers in silicon carbide monitored with deep level transient spectroscopy," *Phys. Status Solidi A*, vol. 162, pp. 199–225, Jul. 1997.

[30] C. Hemmingsson *et al.*, "Deep level defects in electron-irradiated 4H SiC epitaxial layers," *J. Appl. Phys.*, vol. 81, p. 6155, Jan. 1997.

[31] L. Storasta, J. P. Bergman, E. Janzén, J. Lu, and A. Henry, "Deep levels created by low energy electron irradiation in 4H-SiC," *J. Appl. Phys.*, vol. 96, p. 4909, Jun. 2004.

[32] W. C. Mitchel, W. D. Mitchell, H. E. Smith, G. Landis, S. R. Smith, and E. R. Glaser, "Compensation mechanism in high purity semi-insulating 4*H*-SiC," *J. Appl. Phys.*, vol. 101, Mar. 2007, Art. no. 053716.

[33] M. V. S. Chandrashekhar, I. Chowdhury, P. Kaminski, R. Kozlowski, P. B. Klein, and T. Sudarshan, "High purity semi-insulating 4H-SiC epitaxial layers by defect-competition epitaxy: Controlling Si vacancies," *App. Phys. Express*, vol. 5, no. 2, 2012, Art. no. 025502.